Analyst

ROYAL SOCIETY OF CHEMISTRY

PAPER

View Article Online
View Journal | View Issue

Cite this: *Analyst*, 2025, **150**, 3918

A positively charged sensor array for identification of microorganisms using fluorescence response patterns†

Yufan Ma,[a,b] Guoyang Zhang,[b] Xuefei Wang, *[c] Sio-Long Lo*[d] and Zhuo Wang *[b]

Microorganisms, such as bacteria and fungi, are ubiquitous and closely related to human life and health. The identification of microorganisms is especially important in the diagnosis of diseases. Herein, three positively charged tetraphenylethylene derivatives (**PCTs**) were successfully synthesized and used to form a sensor array (**PCTs-Sa**) to identify microorganisms. The three aggregation-induced luminogens (AIEgens) have different cationic groups, multi-color emission and hydrophobicity. By studying the binding energies of phospholipid bilayers and peptidoglycan bilayers, the interaction mechanisms between **PCTs** and different microorganisms were explored. **PCTs** and phospholipid bilayers exhibited different binding energies, resulting in differences in fluorescence imaging. They interacted with microorganisms to produce unique differential fluorescence responses. Through principal component analysis and a support vector machine with 100% accuracy, a variety of microorganisms were identified, including Gram-positive bacteria, Gram-negative bacteria and fungi, spherical bacteria with similar morphology, different mixtures of microorganisms and various concentrations of *Staphylococcus aureus*. This work provides a method with rapid response, high accuracy, high-throughput and no additional washing steps to identify microorganisms.

Received 17th April 2025,
Accepted 9th July 2025

DOI: 10.1039/d5an00439j

rsc.li/analyst

Introduction

Microorganisms are closely related to our life and also have some negative effects on public health. Some serious diseases are caused by microorganism infections, including sepsis,[1] encephalitis,[2] lung infection,[3] and even some cancers.[4] The rapid and accurate diagnosis of infectious diseases is crucial and sometimes plays a role in determining life and death.[5] The convenient and reliable identification of microorganisms can enable effective identification of the types of microorganisms and appropriate treatment to control the progression of diseases.[6–9] Traditional bacteria analysis methods include the plate counting method, polymerase chain reaction (PCR),[10] enzyme linked immunosorbent assay (ELISA),[11] mass spectrometry[12] and so on.[13] Sensing elements based on biomarkers have attracted extensive attention, including antibody–antigen, bacteriophages, enzymes, antibiotics, surface receptors, metabolic markers, antimicrobial peptides and so on.[14–18] Sensing elements interact with microbial targets to generate signals, but the types of biomarkers are limited, which imposes certain limitations on microbial identification. The current methods for the identification of microorganisms have some disadvantages. Therefore, the development of rapid and reliable analysis methods is essential.

Based on the "chemical nose/tongue" strategy, recently, fluorescent and colorimetric array sensing technology has been widely used in microbial discrimination analysis. Various materials have been employed, including gold nanoclusters,[19] quantum dots,[20] carbon dots,[21] conjugated polymers,[22] biological molecules[23] and other fluorescent nanomaterials.[24–27] The types and characteristics of different sensor arrays are summarized in Table S1.† Aggregation-induced emission luminogens (AIEgens) exhibit obvious enhanced emission in the aggregate state.[28] AIEgens offer low background signals and high signal-to-noise ratios in biological imaging,[29–33] which can greatly improve the accuracy and sensitivity of the sensor

[a]*Hebei Province Key Laboratory of Sustained Utilization and Development of Water Recourses, School of Water Resources and Environment, Hebei GEO University, Shijiazhuang 050031, China*
[b]*State Key Laboratory of Chemical Resource Engineering, College of Chemistry, Beijing University of Chemical Technology, Beijing 100029, China. E-mail: wangzhuo77@mail.buct.edu.cn*
[c]*China School of Chemical Science, University of Chinese Academy of Sciences, Beijing 100049, China. E-mail: wangxf@ucas.ac.cn*
[d]*Faculty of Information Technology, Macau University of Science and Technology, Taipa, Macau 999078, China. E-mail: sllo@must.edu.mo*

† Electronic supplementary information (ESI) available. See DOI: https://doi.org/10.1039/d5an00439j

array. The AIEgen sensor array, with its advantages of high sensitivity, rapid response, and designable chemical structure,[34–37] is capable of generating differential fluorescence responses, which allows for the discrimination of microorganisms.[38–43] Currently, there are few sensing elements designed specifically based on the different interactions between probes and membranes.

In previous work, we found that compared with uncharged and negatively charged AIEgens, positively charged AIEgens show good imaging with bacteria.[44] The different cell membranes of microorganisms may play an important role during imaging. The cell walls of Gram-negative bacteria (G^-), Gram-positive bacteria (G^+) and fungi are negatively charged, but have different surface structures and chemical compositions. G^- have a dense outer membrane as a barrier function, which can effectively prevent molecules from entering bacteria. G^+ have a loose and porous cell wall, which is a thick layer of highly cross-linked peptidoglycan located outside the plasma membrane.[45] Fungi are eukaryotes with typical cell walls, mainly composed of β-glycan, chitin, and mannoprotein.[46] The different structures of the cell walls and chemical compositions of microorganisms enable the design concept of probes to distinguish among them.

In this work, three **PCTs** with different positively charged groups, multi-color emission and hydrophobic properties were designed to realize the fluorescent data pattern with different microorganisms (Scheme 1A). We constructed the models of the bacterial wall and studied the binding energy of phospholipid bilayers and peptidoglycan layers with different positively charged molecules. **PCTs** exhibited distinct emission behavior with G^-, because **PCTs** had obviously different binding energies with phospholipid bilayers. Meanwhile, for G^+, the fluorescence of **PCTs** was similar to some degree, and the calculation data indicated that the binding energies with peptidoglycan were similar. G^+ have no phospholipid bilayers outside. **PCTs** had different interactions with microorganisms and produced different fluorescence responses. **PCTs** showed excellent photostability to ensure a reliable database (Scheme 1B). Through Principal Component Analysis (PCA) and Support Vector Machine (SVM) analysis, the recognition of G^+, G^- and fungi can be carried out successfully (Scheme 1C).

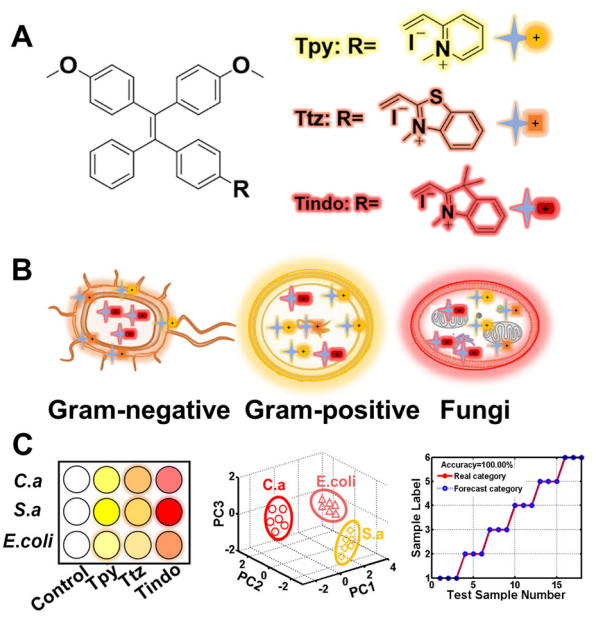

Scheme 1 (A) The chemical structure of **PCTs**. (B) The **PCTs** interact with different microorganisms to produce differential fluorescence responses. (C) The schematic diagram of **PCTs-Sa** for achieving microbial identification.

Experimental section

Materials and instruments

All raw materials and solvents were analytically pure and purchased from commercial channels. Nine types of microorganisms were used, including *Escherichia coli* (*E. coli*), *Staphylococcus aureus* (*S.a*), *Staphylococcus epidermidis* (*S.e*), *Pseudomonas aeruginosa* (*P.a*), *Bacillus subtilis* (*B.s*), *Candida albicans* (*C.a*), *Staphylococcus haemolyticus* (*S.ha*), *Staphylococcus hominis* (*S.ho*) and *Staphylococcus suis* (*S.s*), purchased from Beijing Tiantan Hospital. A laser confocal microscope (Leica Microsystem Leica SP8) was used to record the laser confocal images. Using a black 96-well plate, the fluorescence intensity of the probe before and after the addition of microorganisms was measured on a microplate reader (Thermofisher Varioskan Flash).

Culture and preparation of microorganisms

The individual *E. coli* colonies on the solid medium were transferred to 10 mL of liquid LB medium and cultured in a shaking incubator for 12 h. The concentration was determined by measuring the optical density at 600 nm (OD_{600}) using a UV spectrophotometer. The microorganisms were diluted to OD_{600} = 0.5 and transferred to a 1.5 mL centrifuge tube. The microorganisms were centrifuged at 8000 rpm for 3 min. After centrifugation, the supernatant was removed and washed three times with phosphate buffer solution (PBS) to remove the medium. The precipitated *E. coli* was dispersed again in PBS for later use. Other microorganisms were cultured under the same conditions and procedures as *E. coli*.

Computational methods

The geometry optimization of **Tpy**, **Ttz** and **Tindo** was performed using the Gaussian 09 software package with the PM6 semiempirical method. Molecular dynamics (MD) simulations were employed to probe the interactions between the **PCTs** and phospholipid bilayer/peptidoglycan layers. The process of dynamics was performed using Materials Studio (MS) software with the Forcite module and Universal Force Field (UFF). The simulation temperature was set to 298.15 K, which was controlled by the Andersen method. Long-range Coulomb interactions were calculated by the Ewald summation technique, and van der Waals interactions were obtained using the

"spline-cutoff" method. 5 ns MD simulations were carried out in an isothermal-isovolumetric (NVT) ensemble with a time step of 1 fs. The binding energy (E_{bind}) of **PCTs** to phospholipid bilayers/peptidoglycan layers can be defined as follows: $E_{bind} = E_{A/M} - (E_A + E_M)$, where $E_{A/M}$ is the total energy after binding, E_M is the energy of the phospholipid bilayer or peptidoglycan layer, and E_A is the energy of **Tpy**, **Ttz** or **Tindo**.

Fluorescence intensity of microorganisms incubated with PCTs

The **PCTs** were dissolved in dimethyl sulfoxide to prepare a solution with an initial concentration of 10^{-2} M. A small amount of the solution was diluted to 40 μM with PBS for later use. 1 mL of the treated microorganism solution and an equal amount of probe solution were added to the sterilized centrifuge tube and incubated at room temperature for 15 min. The microorganisms were dispersed evenly in the solution and transferred to a cuvette. Finally, fluorescence intensity was measured using a fluorescence spectrometer.

Confocal microscope imaging

200 μL of the treated microorganism solution and an equal amount of probe solution (40 μM) were added to the sterilized centrifuge tube and incubated at room temperature for 15 min. 10 μL of stained microorganisms was transferred to a clean glass slide and fixed with a coverslip. The images were collected under a confocal laser scanning microscope using 405 nm and 488 nm lasers and a 100× oil lens.

Identification of microorganisms

100 μL of microorganisms was transferred to a black 96-well plate and then 100 μL of the diluted probe solution (40 μM) was added. The final volume of each well was 200 μL. After shaking for 30 s, the mixture was incubated with a shaker at 37 °C for 15 min. The fluorescence intensity was measured at various excitation/emission ($\lambda_{ex}/\lambda_{em}$) wavelengths, $\lambda_{ex}/\lambda_{em}$ = 405/575 nm, 405/625 nm, 405/675 nm, 488/575 nm, 488/625 nm, and 488/675 nm on a microplate reader. The probe solution free of microorganisms was treated as the control experiment under the same conditions. The relative fluorescence intensity (I/I_0) of the probe before and after incubation with microorganisms was calculated using Microsoft Excel software, where I is the fluorescence intensity of the probe after adding microorganisms and I_0 is the fluorescence intensity of the probe without microorganisms. The relative fluorescence intensity I/I_0 obtained was introduced into the mathematical analysis through MATLAB software and analysed by PCA to identify and analyse the microorganism. The same steps were used to identify mixed and different concentration samples.

Unknown identification

Fluorescence cross-response analysis was performed on unknown blind samples. Using MATLAB software, the training set and the unknown sample set were tested by the SVM statistical method to obtain the unknown sample category. Compared with pre-labelled microorganism categories, the prediction accuracy of unknown samples can be obtained.

Results and discussion

Synthesis and characterization of PCTs

Due to the negative charge on the cell membrane, probes with positive charges are easier to image microorganisms. **PCTs** (**Tpy**, **Ttz**, and **Tindo**) were designed based on the properties of the conjugated system of the target molecule, the positive charges, the molecular polarity, and the oil–water partition coefficient. **PCTs** were prepared through a series of chemical reactions (Schemes S1–S3, ESI†). Firstly, TBr was synthesized according to the McMurray reaction. Then, *n*-BuLi was used to convert –Br to –CHO and synthesize TCHO. Finally, through the Knoevenagel reaction, TCHO was reacted with 1,2-dimethylpyridinium-1-iodide, 2,3-dimethylbenzo [*d*] thiazole-3-iodide and 1,2,3,3-tetramethyl-3*H*-indole-1-iodide to yield **PCTs**. The chemical structures of **PCTs** were analyzed and characterized by ^{1}H NMR, ^{13}C NMR, ESI-MS and high resolution mass spectrometry (HRMS) (Fig. S1–S12†). **PCTs** carry a positive charge on pyridine, thiazole and indole, respectively. The physical, chemical, and spectral characteristics of **PCTs** were characterized and recorded (Fig. 1 and Table S2†).

Introducing different electron-donating groups into the TPE skeleton can adjust the energy gap between the highest occu-

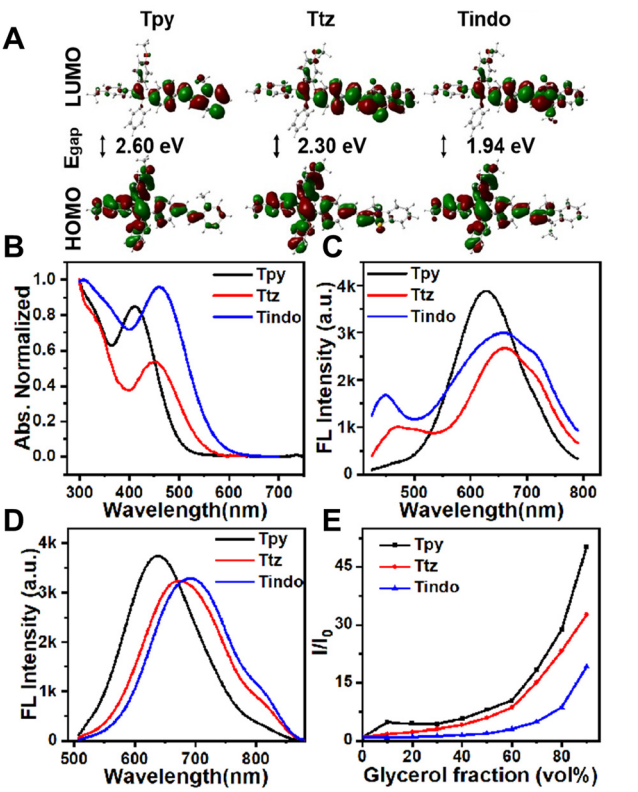

Fig. 1 Spectral properties of **PCTs**. (A) The positive potential and LUMO–HOMO distribution of **PCTs**. (B) The normalized absorption spectra of **PCTs** (20 μM) in 65% glycerol solution. The fluorescence spectra of 20 μM **PCTs** in 65% glycerol solution (C) λ_{ex} = 405 nm and (D) λ_{ex} = 488 nm. (E) The relative fluorescence intensity (I/I_0) of 20 μM **PCTs** under the maximum emission peak in different glycerol ratios.

pied molecular orbital (HOMO) and the lowest unoccupied molecular orbital (LUMO) of the probes. The electron cloud distribution and energy gap (E_{gap}) between the HOMO and LUMO were calculated using the DFT B3LYP-D3/6-31G+(d,p) method. The lower the E_{gap}, the more red-shifted the emission wavelength. The E_{gap} values of **Tpy**, **Ttz**, and **Tindo** were calculated to be 2.60, 2.30 and 1.94 eV, respectively (Fig. 1A). Therefore, **Tpy** exhibits the shortest fluorescence emission wavelength, while **Tindo** exhibits the longest fluorescence emission wavelength.

The spectral properties were studied and characterized. The UV-vis spectra showed that **PCTs** had different excitation wavelengths (Fig. 1B). The maximum absorption peaks of **PCTs** were at 405 nm, 450 nm and 470 nm, respectively. The changes in the absorption peaks were mainly due to the differences between the electron donor and acceptor units. The absorption peak of the structure with more conjugated systems exhibited a red shift. 405 nm and 488 nm were selected as excitation wavelengths for recording the emission spectra. As shown in Fig. 1C and D, the fluorescence intensity of **PCTs** differed significantly at excitation wavelengths of 405 nm and 488 nm. **PCTs** showed multi-color fluorescence emission, and the maximum fluorescence emission peaks were at 627 nm (**Tpy**), 655 nm (**Ttz**) and 675 nm (**Tindo**), respectively. Tetraphenylethylene (TPE) is a typical molecule with AIE properties. The AIE properties of **PCTs** were characterized in glycerol solutions of different proportions. **PCTs** exhibited weak emission in PBS, and fluorescence emission gradually increased with the increase of the glycerol ratio (from 0 to 90%) (Fig. 1E and Fig. S13†). By calculating the relative fluorescence intensity (I/I_0, where I_0 and I are the maximum fluorescence intensity of **PCTs** in PBS and different glycerol ratios) of **PCTs** in PBS and after adding different ratios of glycerol, the fluorescence intensity of **PCTs** differed significantly when the same ratio of glycerol was added. The fluorescence in the 90% glycerol solution increased by 49.01 (**Tpy**), 32.67 (**Ttz**), and 19.22 (**Tindo**) times, respectively (Fig. 1E). Due to the aggregation of molecules in glycerol solution, intramolecular rotation was restricted, resulting in the activation of fluorescence intensity and exhibiting typical AIE characteristics.

Meanwhile, **PCTs** have different hydrophilic and hydrophobic properties. The log P of **PCTs** was calculated using ALOGPs 2.1. The Clog P values of **Tpy**, **Ttz** and **Tindo** are 3.70, 4.72 and 4.74, respectively (Table S2†). **PCTs** present various chemical structures, different positive potentials, LUMO–HOMO distributions, multi-color fluorescence emission, and hydrophobicity. The imaging profiles of positive **PCTs** need to be studied to illustrate the response of **PCTs** to microorganisms. The fluorescence intensity of **PCTs** is co-modulated by multiple factors including hydrophobic, electrostatic, hydrogen bonding, AIE properties, and microbial microenvironments, leading to differential fluorescence responses during the interaction between **PCTs** and microorganisms. The electrostatic attraction is a strong force that brings two oppositely charged species together; the AIEgens bearing a positively charged pendant showed light-up characteristics upon binding with the negative surfaces of microorganisms.[40] Hydrophobic and microbial microenvironments affect the fluorescence intensity during the interaction between AIEgens and microorganisms.[42] Meanwhile, according to the fluorescent properties of the **PCTs**, multichannel identification and discrimination analysis of various microorganisms were realized.

Co-localization and mechanism of PCTs

DAPI is a commercial dye that stains DNA in the cytoplasm. By the co-localization of **PCTs** and DAPI, we can see whether **PCTs** can enter the microbial cytoplasm. The results of confocal imaging showed that when incubated with *E. coli* (G^-), **Tpy** stained the cell wall and cytoplasm (Fig. 2A). **Ttz** mainly stained the cell wall and part of the cytoplasm (Fig. 2B). The staining of **Tindo** and DAPI was highly co-localized and stained the cytoplasm (Fig. 2C). For G^+, all **PCTs** (red channel) presented good colocation with DAPI (green channel) (Fig. 2D–F). Compared with G^-, **PCTs** entered the cytoplasm of G^+ more quickly. The dense outer wall of G^- provides additional protection, which inhibits the entering of **PCTs**. The outer wall of G^+ is composed of loose and porous peptidoglycan and negatively charged teichoic acid. The positively

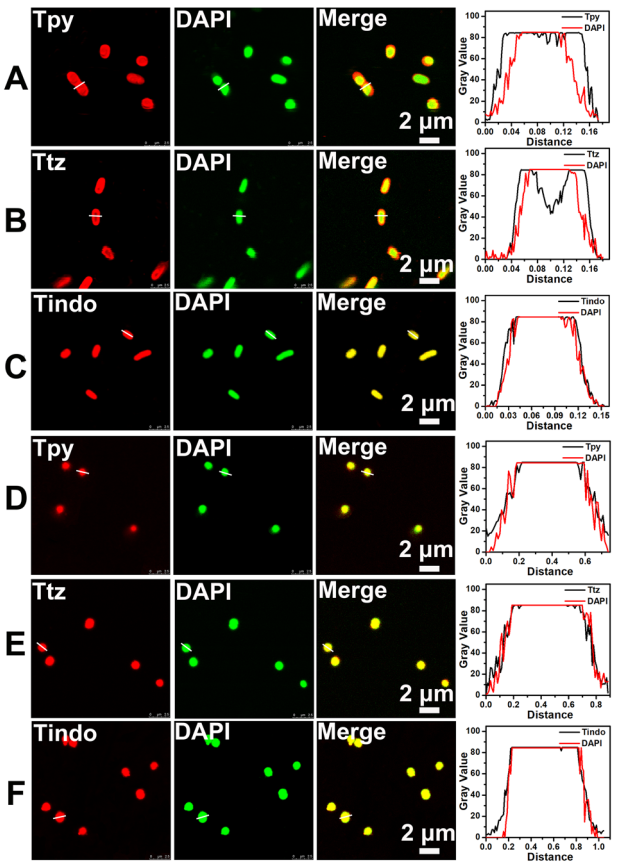

Fig. 2 Co-localization of **PCTs** with microorganisms. Confocal fluorescence images of **PCTs** and DAPI with (A–C) *E. coli* and (D–F) *S.a*. The scale bar is 2 μm. $\lambda_{Ex}/\lambda_{Em}$ of Tpy, Ttz, Tindo and DAPI is 405/550–700 nm, 405/550–700 nm, 488/550–700 nm and 405 nm/430–490 nm, respectively.

charged **PCTs** can enter G^+ quickly and emit strong fluorescence.

We studied the interaction of the probes and the cell wall by theoretical simulation. The dense cell wall of G^- is a phospholipid bilayer, and the loose cell wall of G^+ is peptidoglycan. For stimulating the cell wall of G^-, the outer membrane was approximately represented by a model of a 6.4 nm × 6.4 nm phospholipid bilayer (Fig. S14D†). For simulating the cell wall of G^+, a model of four parallel peptidoglycan layers (6.9 nm × 5.0 nm for each layer) was constructed (Fig. S14E†). Molecular dynamics (MD) simulations were employed to probe the interactions of **PCTs** and phospholipid bilayer/peptidoglycan layers. The last snapshot of the dynamics was selected to observe the hydrogen bond interactions between **PCTs** and phospholipid bilayer/peptidoglycan layers (Fig. 3 and Table S3†). The results of binding energy are shown in Table S4.†

The hydrogen bonds between **PCTs** and phospholipid bilayers/peptidoglycan layers create additional interactions between the probe and the cell wall, allowing the probe to enter the microorganism, inhibiting molecular rotation and emitting fluorescence. The G^- cell wall is composed of a dense phospholipid bilayer, in which negatively charged phosphate groups attract positively charged **PCTs**. **Tpy** had a low binding energy (−4.08 kcal mol^{-1}), and the hydrophilicity may reduce **Tpy**'s permeability through the outer wall phospholipid bilayer and lead to partial embedding of **Tpy** in the outer layer of the cell wall. **Ttz** had a high binding energy (−43.54 kcal mol^{-1}), causing aggregation and limiting molecular rotation to emit fluorescence. **Tindo** had a moderate binding energy (−13.54 kcal mol^{-1}), and the hydrophobicity of the indole group enabled it to cross the cell membrane and enter the cytoplasm to generate fluorescence. The outer wall of G^+ was composed of loose and porous peptidoglycan and negatively charged teichoic acid. The binding energy values of **PCTs** and peptidoglycan were relatively low and similar. The binding energies of the three probes were −0.74 kcal mol^{-1}, −0.78 kcal mol^{-1} and −0.80 kcal mol^{-1}, respectively. Meanwhile, the negatively charged teichoic acid attracted the positively charged **PCTs**, allowing the probes to enter the microorganism for imaging, laying the foundation for microorganism identification. Hydrogen bonds between **PCTs** and the phospholipid bilayer/peptidoglycan layer can anchor the probes more firmly to the microbial surface. **PCTs** exhibit typical AIE properties, and the formation of hydrogen bonds inhibits the free rotation of probe molecules, thereby enhancing the fluorescence intensity.[47]

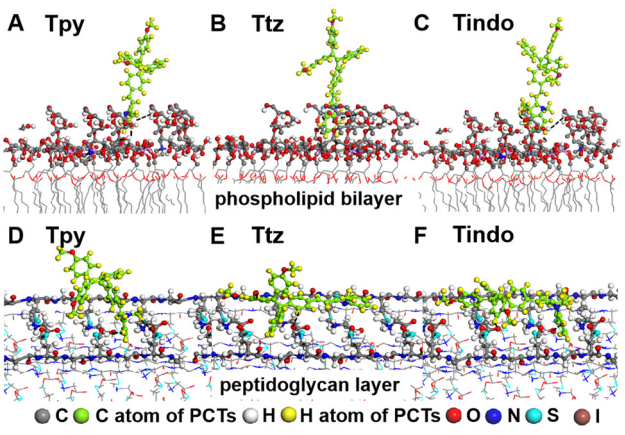

Fig. 3 The interactions of **PCTs** (Tpy, Ttz, and Tindo) and the phospholipid bilayer (A–C)/peptidoglycan layer (D–F) determined by MD simulations.

Staining and imaging of PCTs

The three dyes of **PCTs** showed different interactions with the cell wall of bacteria, which endowed them with the distinguished fluorescence imaging response. The fluorescence spectra of 5 types of microorganisms with **PCTs** were recorded, including G^- (*Escherichia coli* (*E. coli*) and *Pseudomonas aeruginosa* (*P.a*)), G^+ (*Staphylococcus aureus* (*S.a*) and *Staphylococcus epidermidis* (*S.e*)) and fungi (*Candida albicans* (*C.a*)). As shown in Fig. S15 and S16,† when **PCTs** were incubated with microorganisms, the fluorescence intensity changed to varying degrees. Taking **Ttz** as an example, after incubating with microorganisms, the fluorescence intensity change of **Ttz** followed the trend: *S.a* > *C.a* > *S.e* > *E. coli* > *P.a*. The fluorescence intensity changes of 6 types of common microorganisms after incubation with **PCTs** were different. Meanwhile, the maximum emission wavelengths of **PCTs** do not change a lot.

PCTs were used to image 6 types of common microorganisms using a confocal laser scanning microscope (CLSM), including G^- (*E. coli* and *P.a*), G^+ (*S.a*, *S.e*, and *B.s*) and fungi (*C.a*). **PCTs** can stain different microorganisms to produce different fluorescence responses (Fig. 4). The fluorescence intensity of *S.a* stained with **PCTs** was higher and exhibited varying degrees of fluorescence enhancement. The fluorescence of *E. coli* stained with **Tindo** and **Ttz** was relatively weaker than that of other probes. **PCTs** were used to image 5 types of similarly shaped spherical bacteria, including 4 kinds of human-origin bacteria (*S. aureus* (*S.a*), *S. epidermidis* (*S.e*), *S. haemolyticus* (*S. ha*), and *S. hominis* (*S. ho*)) and 1 kind of porcine-derived bacteria (*S. suis* (*S. s*)). **PCTs** can stain these spherical bacteria, and different microorganisms produce different fluorescence responses (Fig. S17†). After staining with *S.e*, the fluorescence intensity of **Tpy** and **Ttz** was lower than that of **Tindo**. When **PCTs** were stained with G^+, they produced strong fluorescence. The binding capabilities of **PCTs** with different microorganisms caused a change in fluorescence. The confocal images of **PCTs** with 6 types of common microorganisms and 5 types of spherical microorganisms show that **PCTs** can not only effectively stain microorganisms, but also display differential fluorescence response signals.

In the imaging process, long-term tracking and real-time imaging were important as they can broaden the application range of probes in microbial research. The photostability of **PCTs** with G^- (*E. coli*) and G^+ (*S.a*) was further studied by continuous light irradiation. After 900 s of light irradiation, the fluorescence intensity of **PCTs** remained above 80% in both G^-

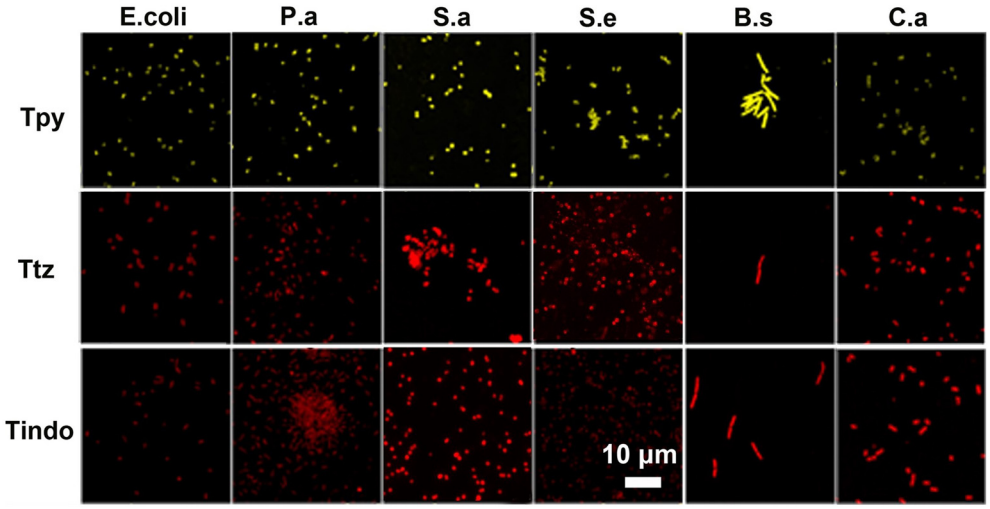

Fig. 4 CLSM images of 20 μM **PCTs** stained with 6 kinds of microorganisms. The different colors (orange and red) are consistent with the maximum emission wavelength. λ_{ex} = 405 nm and λ_{em} = 450–600 nm (Tpy); λ_{ex} = 488 nm and λ_{em} = 510–800 nm (Ttz and Tindo). The scale bar is 10 μm.

and G^+ (Fig. S18†). **PCTs** had good photobleaching resistance, long-term tracking and real-time imaging capabilities. The diverse fluorescence responses and good photostability of **PCTs** laid the foundation for building a sensor array-**PCTs-Sa** to identify microorganisms.

PCTs-Sa for microorganism identification

Fluorescence responses of PCTs-Sa. In the process of exploring **PCTs-Sa** for microorganism identification, fluorescence data were recorded using a microplate reader. Based on the fluorescence imaging results, we selected two optimal excitation wavelengths of **PCTs** (λ_{ex}: 405 nm and 488 nm) for data recording. According to the previous spectra, we selected the corresponding three emission wavelengths (λ_{em}: 575 nm, 625 nm, and 675 nm), and the excitation was set at 405 nm and 488 nm. The relative fluorescence intensity (I/I_0) of **PCTs** was used to characterize the differential fluorescence response patterns. As shown in Fig. 5A, B, E, and F and Fig. S19 and S20,† due to the difference in the binding capacity of the **PCTs** and microorganisms, each probe produced different fluorescence response patterns after incubation with different microorganisms. This clearly proved the possibility that **PCTs** can identify microorganisms.

Microorganism identification by PCTs-Sa. 6 types of microorganisms were selected for analysis, including G^- (*E. coli* and *P.a*), G^+ (*B.s*, *S.a* and *S.e*) and fungi (*C.a*). Based on the negatively charged residues and the external hydrophobic groups of the microorganisms, **PCTs** showed different interactions and produced various fluorescence responses (Fig. 5A, B and Fig. S19†). **PCTs-Sa** was used to obtain the fluorescence pattern for the following data analysis. The collected response data were subjected to principal component analysis (PCA). PCA used the idea of dimensionality reduction to convert multiple indicators into a few comprehensive indicators (principal components) to simplify the problem. Among the obtained data components, the cumulative contribution of the first three principal components accounts for the main component. Therefore, the first three principal components were selected to obtain the principal component score map. In the score chart, each point represented a type of bacteria. Sample points with similar characteristics were concentrated in the same area. The farther the distance between the sample points presented, the greater the difference between the samples. By PCA analysis, a three-dimensional PCA score map of different common microorganisms by **PCTs-Sa** was obtained (Fig. 5C). **PCTs-Sa** could identify these different microorganisms with 100% accuracy.

Repeatability is a major challenge for a sensor array. Unknown samples of 6 types of microorganisms (6 × 3 repetitions = 18) were used to verify the predictive ability of **PCTs-Sa**, and Support Vector Machine (SVM) analysis was performed. SVM is a supervised learning model for classification, regression and prediction. To predict the sample category, a set of training samples was tested, and the samples were marked as different categories by SVM (red line in Fig. 5D). The unknown samples were tested to form a dataset and the same mapping was performed by SVM to obtain a predicted category (blue line in Fig. 5D). By comparing the predicted category with the actual category, the category of the sample could be predicted, and then the predictive ability of **PCTs-Sa** for unknown samples could be obtained. Through SVM, **PCTs-Sa** could predict unknown samples with 100% accuracy (Fig. 5D). Therefore, **PCTs-Sa** could effectively distinguish G^-, G^+ and fungi.

As shown in Fig. S20A,† the confusion matrix results indicate that the classification performance is excellent. To further calculate other evaluation metrics for the method, the precision, recall, and F1 score were calculated, all of which achieved 100%. This indicates its effectiveness in correctly identifying positive and negative instances in the dataset.

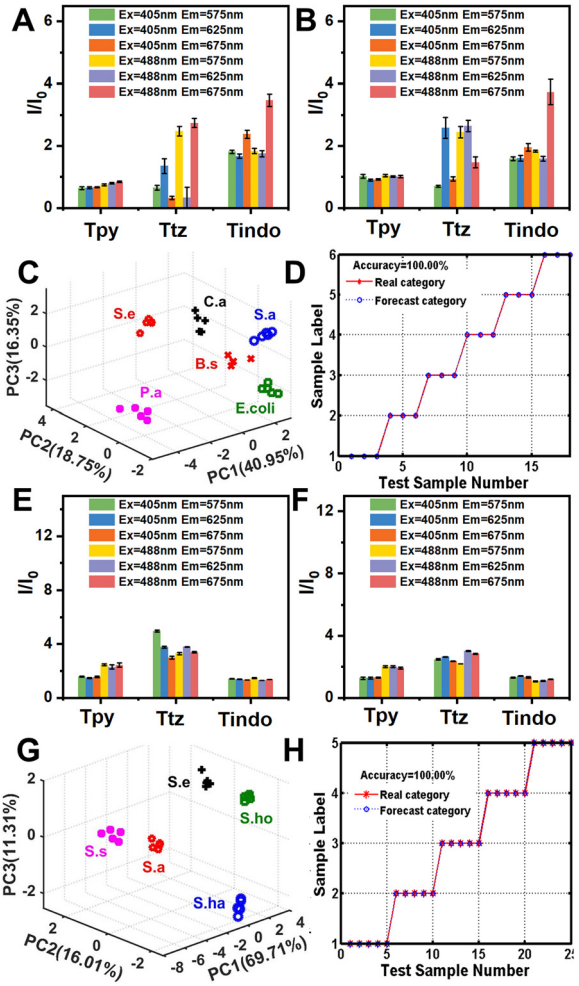

Fig. 5 Differential fluorescence responses of **PCTs-Sa** incubated with (A) *C.a*, (B) *E. coli*, (E) *S.a*, and (F) *S.s*. The PCA score chart of differential fluorescence response analysis of (C) common microorganisms and (G) spherical bacteria with a similar appearance. The SVM analysis results of unknown samples: (D) common microorganisms and (H) spherical bacteria with a similar morphology. The error bar in ABEF shows the standard deviation of five independent measurements.

These metrics suggest that the model is well-suited for the classification task at hand.

Spheroid microorganism identification by PCTs-Sa. To further verify the versatility of **PCTs-Sa**, we tested the ability of **PCTs-Sa** to recognize 5 types of spheroid bacteria with similar morphology, including 4 types of human-origin staphylococci (*S.a*, *S.e*, *S.ha*, and *S.ho*) and one type of porcine-derived *Staphylococcus* (*S.s*). The fluorescence response signals of **PCTs-Sa** incubated with these spherical bacteria were significantly different (Fig. 5E, F and Fig. S21†). The spherical bacteria incubated with **PCTs** produced fluorescence response patterns. PCA was performed on **PCTs** (Fig. 5G), and the 5 types of spherical bacteria with a similar morphology and relatively small structural differences could be clearly distinguished. Meanwhile, the data points of porcine-derived and human-derived *Staphylococcus* were well separated in the pattern. Unknown samples of these spherical bacteria (5 × 5 repetitions = 25) were used to verify the predictive ability of **PCTs-Sa**. Through SVM, **PCTs-Sa** presented 100% accuracy for unknown samples (Fig. 5H). The precision, recall, and F1 score were calculated, all of which reached 100% (Fig. S20B†). Therefore, **PCTs-Sa** could identify the 5 types of human origin and porcine-derived spherical bacteria with a similar morphology.

Complex sample identification by PCTs-Sa. In practical applications, we often face the analysis of samples with several mixed microorganisms. To evaluate the potential of **PCTs-Sa** for complex samples, we mixed 2 or 3 types of microorganisms for analysis. 5 kinds of microorganisms (*E. coli*, *P.a*, *S.a*, *S.e* and *C.a*) were selected to randomly produce six mixtures of bacteria in equal proportions, including a mixture of 3 or 2 kinds of microorganisms (such as 33.3% *E. coli* + 33.3% *P.a* + 33.3% *C.a*, 33.3% *S.a* + 33.3% *S.e* + 33.3% *C.a*, 33.3% *E. coli* +

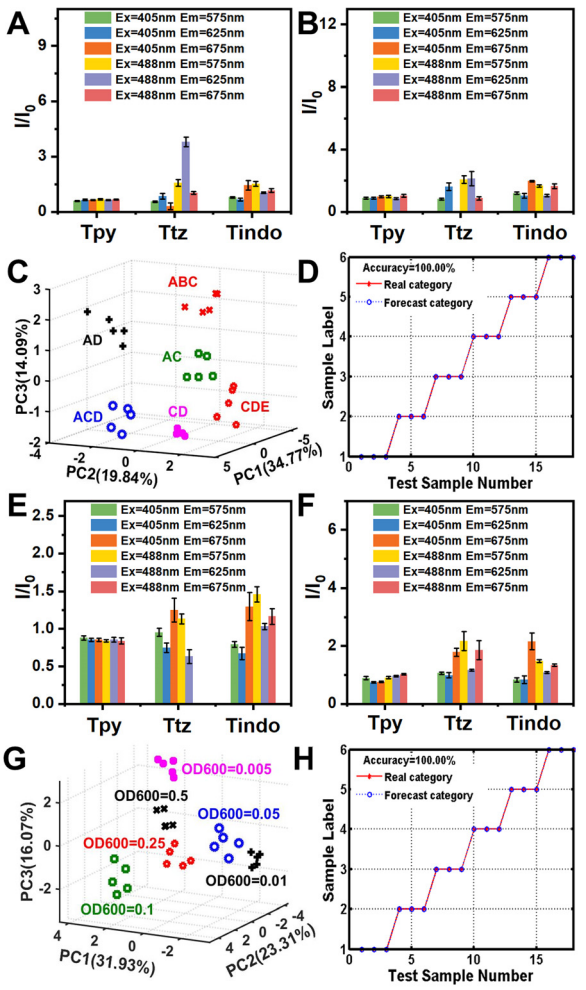

Fig. 6 Differential fluorescence responses of **PCTs-Sa** incubated with (A) AC, (B) ACE, (E) OD_{600} = 0.005, and (F) OD_{600} = 0.5. The PCA score chart of differential fluorescence response analysis of (C) complex samples and (G) various concentrations of *S.a*. The SVM analysis results of unknown samples: (D) complex samples and (H) various concentrations of *S.a*. A is *E. coli*, B is *P.a*, C is *C.a*, D is *S.a*, and E is *S.e*. The error bar in ABEF shows the standard deviation of five independent measurements.

33.3% *S.a* + 33.3% *C.a*, 50% *S.a* + 50% *C.a*, 50% *E. coli* + 50% *C.a* and 50% *E. coli* + 50% *S.a*, respectively). When incubated with the different mixed samples, **PCTs-Sa** captured the combinatorial responses of various species in the mixture, generating differential fluorescence response patterns (Fig. 6A and B and Fig. S22†). PCA was used to obtain the principal component score map (Fig. 6C). 6 mixed samples were separated from each other, and the data points of the same sample are clustered with each other. Using 6 unknown samples of mixed bacteria (6 × 3 repetitions = 18), SVM obtained 100% prediction accuracy (Fig. 6D). The precision, recall, and F1 score were calculated, all of which reached 100% (Fig. S23A†). Therefore, **PCTs-Sa** can effectively identify mixed samples.

Various concentration sample identification by PCTs-Sa. At the early stage of infection, one of the important problems is that the number of microorganisms is too low. So accurate identification and quantitative analysis of the low number of microorganisms are extremely important. In order to further verify that **PCTs-Sa** not only can distinguish mixed samples, but also has the ability of quantitative detection, *S.a* was selected as an example and quantitative analysis of different concentrations of the bacteria (OD_{600} = 0.5, 0.25, 0.1, 0.05, 0.01, and 0.005) was performed. **PCTs-Sa** and 6 different concentrations of *S.a* had various fluorescence response patterns (Fig. 6E, F and Fig. S24†). With the enhancement of the concentration, the fluorescence intensity gradually increased. Even at the lowest concentration (OD_{600} = 0.005), **PCTs-Sa** could be identified with 100% accuracy (Fig. 6G). SVM analysis was performed on the fluorescence response data sets of unknown samples with different concentrations of *S.a* (6 × 3 repetitions = 18), which showed that **PCTs-Sa** had 100% ability to identify unknown samples (Fig. 6H). The precision, recall, and F1 score were calculated, all of which reached 100% (Fig. S23B†). Therefore, **PCTs-Sa** could effectively quantify bacteria. **PCTs-Sa** had 100% recognition accuracy in complex samples and samples with different microorganism concentrations, which greatly promotes its application.

Conclusions

In summary, three probes with different cations were successfully constructed for the identification of microorganisms. **PCTs** exhibited aggregate-induced fluorescence with microorganisms. **PCTs** stained different microorganisms and produced unique differential fluorescence response patterns. By studying the binding energy of phospholipid bilayers and peptidoglycan bilayers, the interaction mechanism between **PCTs** and microorganisms was explored. Due to the dense outer wall of G^-, **PCTs** and phospholipid bilayers had different binding energies, resulting in differences in fluorescence imaging. The sensor array realized the identification of different microorganisms with 100% accuracy, including typical microorganisms and spherical bacteria with a similar morphology. Meanwhile, the sensor array was suitable for analyzing complex situations, including a mixture of multiple microorganisms and different concentrations of bacteria, and could accurately identify bacteria at very low concentrations (OD_{600} = 0.005). It can provide timely and reliable information for the identification of typical microorganisms.

Author contributions

Yufan Ma: investigation, data curation, writing – original draft, and funding acquisition; Guoyang Zhang: formal analysis, visualization and validation; Xuefei Wang: methodology, software, and writing – review & editing; Sio-Long Lo: resources, methodology, validation, and supervision. Zhuo Wang: project administration, conceptualization, writing – review & editing, and funding acquisition.

Conflicts of interest

There are no conflicts to declare.

Data availability

The data supporting this paper have been included as part of the ESI.†

It contains the details of the synthesis of **PCTs**; ^{1}H NMR, ^{13}C NMR, and mass spectra for the compounds; fluorescence intensity spectra of **PCTs**; the geometry optimized structures of phospholipid bilayers and peptidoglycan layers; the fluorescence intensity of **PCTs** in different microorganisms; confocal fluorescence images of spherical bacteria stained with **PCTs**; photostability of **PCTs**; fluorescence images of different microorganisms incubated with **PCTs**; confusion matrix of the evaluation results; types and characteristics of different sensor arrays; properties of **PCTs**; hydrogen bond interactions and binding energy between **PCTs** and phospholipid bilayers/peptidoglycan bilayers.

Acknowledgements

We are thankful for support from the National Pre-research Funds of Hebei GEO University in 2024 (No. KY2024QN06), the National Key Research and Development Program of China (No. 2021YFC2101500), the Natural Science Foundation of Beijing Municipality (No. 7232342 and 8222074), and the Academy of Medical Sciences Newton Advanced Fellowship (No. NAFR13\1015).

References

1 R. A. Weinstein, R. Gaynes and J. R. Edwards, *Clin. Infect. Dis.*, 2005, **41**, 848–854.
2 A. Mailles, J. P. Stahl and K. C. Bloch, *Clin. Microbiol. Infect.*, 2017, **23**, 607–613.

3 R. Mazzolini, I. Rodríguez-Arce, L. Fernández-Barat, C. Piñero-Lambea, V. Garrido, A. Rebollada-Merino, A. Motos, A. Torres, M. J. Grilló, L. Serrano and M. Lluch-Senar, *Nat. Biotechnol.*, 2023, **41**, 1089–1098.
4 N. D. Wolfe, C. P. Dunavan and J. Diamond, *Nature*, 2007, **447**, 279–283.
5 B. Koo, M. G. Kim, K. Lee, J. Y. Kim, S. Lee, S. H. Kim and Y. Shin, *Sens. Actuators, B*, 2023, **380**, 133382.
6 Y. Chen, J. Liu, J. Liu, R. Hu, Y. Yang and X. Zhang, *Chem. Res. Chin. Univ.*, 2024, **40**, 305–310.
7 L. Váradi, J. L. Luo, D. E. Hibbs, J. D. Perry, R. J. Anderson, S. Orenga and P. W. Groundwater, *Chem. Soc. Rev.*, 2017, **46**, 4818–4832.
8 Y. Yu, W. Ni, X. Shi, Y. Bian, H. Li, M. Liu, W. Chen, M. Zhang, S. Jiang, M. Cheng, F. Li, Y. Zhang, Z. Zhang, H. Huang and J. Han, *Anal. Chem.*, 2024, **96**, 14490–14498.
9 L. Zhao, H. Hu, X. Ma, Y. Lyu, Q. Yuan and W. Tan, *Chem. Res. Chin. Univ.*, 2024, **40**, 173–189.
10 M. Maurin, *Expert Rev. Mol. Diagn.*, 2014, **12**, 731–754.
11 N. Xu, W. Wang, F. Chen, W. Li and G. Wang, *BMC Infect. Dis.*, 2020, **20**, 1–7.
12 Z. Zhang, E. Xing, W. Zhao, M. Song, C. Zhang, H. Liu, X. Li and H. Yu, *Analyst*, 2025, **150**, 827–840.
13 R. Weiss, M. Palatinszky, M. Wagner, R. Niessner, M. Elsner, M. Seidel and N. P. Ivleva, *Analyst*, 2019, **144**, 943–953.
14 H. J. Kim and S. J. Choi, *Anal. Methods*, 2020, **12**, 5621–5627.
15 W. L. Zhang, Z. Y. He and L. L. Yi, *Biosens. Bioelectron.*, 2018, **102**, 652–660.
16 P. Dow, K. Kotz, S. Gruszk, J. Holder and J. Fiering, *Lab Chip*, 2018, **18**, 923–932.
17 K. H. Kim, S. J. Park, C. S. Park, S. E. Seo, J. Lee, J. Kim, S. H. Lee, S. Lee, J. S. Kim, C. M. Ryu, D. Yong, H. Yoon, H. S. Song, S. H. Lee and O. S. Kwon, *Biosens. Bioelectron.*, 2020, **167**, 112514.
18 G. W. Xing, W. F. Zhang, N. Li, Q. S. Pu and J. M. Lin, *Chin. Chem. Lett.*, 2022, **33**, 1743–1751.
19 Y. Wu, B. Wang, K. Wang and P. Yan, *Anal. Methods*, 2018, **10**, 3939–3944.
20 H. Yuan, H. Zhao, K. Peng, R. Qi, H. Bai, P. Zhang, Y. Huang, F. Lv, L. Liu, J. Bao and S. Wang, *ACS Appl. Mater. Interfaces*, 2020, **12**, 21263–21269.
21 S. Wang, Y. Zhang, P. Zhuo, Q. Hu, Z. Chen and L. Zhou, *J. Mater. Chem. B*, 2020, **8**, 5877–5882.
22 H. Wang, L. Zhou, J. Qin, J. Chen, C. Stewart, Y. Sun, H. Huang, L. Xu, L. Li, J. Han and F. Li, *Anal. Chem.*, 2022, **94**, 10291–10298.
23 Z. Sun, S. Wu, Y. Peng, M. Wang, M. Jalalah, M. S. Al-Assiri, F. A. Harraz, J. Yang and G. Li, *Chem. Eng. J.*, 2021, **405**, 126707.
24 X. Li, B. Li, R. Liu, Y. Dong and Y. Wu, *Anal. Bioanal. Chem.*, 2021, **413**, 4689–4696.
25 Z. Lu, N. Lu, Y. Xiao, Y. Zhang, Z. Tang and M. Zhang, *ACS Appl. Mater. Interfaces*, 2022, **14**, 11156–11166.
26 M. Zhao, Y. Yan, H. Guo, Y. Zhang, H. Wu, Y. Fang and Y. Liu, *Analyst*, 2022, **147**, 2247–2252.
27 Y. Ma, Y. Li, K. Ma and Z. Wang, *Sci. China:Chem.*, 2018, **61**, 643–655.
28 J. Luo, Z. Xie, J. W. Y. Lam, L. Cheng, B. Z. Tang, H. Chen, C. Qiu, H. S. Kwok, X. Zhan, Y. Liu and D. Zhu, *Chem. Commun.*, 2001, **18**, 1740–1741.
29 P. Chen, G. Zhang, J. Li, L. Ma, J. Zhou, M. Zhu, S. Li and Z. Wang, *Chem. Res. Chin. Univ.*, 2024, **40**, 293–304.
30 Y. Hu, X. Gao, J. Ma, Z. Shangguan, L. Chen, G. Zhang, X. S. Zhang, C. Li, Y. Li and D. Zhang, *Aggregate*, 2025, e735.
31 Y. Huang, G. Zhang, R. Zhao and D. Zhang, *Chem. – Eur. J.*, 2023, **29**, e202300539.
32 Y. Ma, H. Wang, S. Su, Y. Chen, Y. Li, X. Wang and Z. Wang, *Analyst*, 2019, **144**, 3381–3388.
33 J. Mei, Y. Hong, J. W. Y. Lam, A. Qin, Y. Tang and B. Z. Tang, *Adv. Mater.*, 2014, **26**, 5429–5479.
34 Y. Duo, Z. Xiang, G. Gao, G. Luo and B. Z. Tang, *Trends Anal. Chem.*, 2023, **167**, 117252.
35 G. Feng, Y. Yuan, H. Fang, R. Zhang, B. Xing, G. Zhang, D. Zhang and B. Liu, *Chem. Commun.*, 2015, **51**, 12490–12493.
36 J. Liang, B. Z. Tang and B. Liu, *Chem. Soc. Rev.*, 2015, **44**, 2798–2811.
37 Y. Ma, W. Ai, J. Huang, L. Ma, Y. Geng, X. Liu, X. Wang, Z. Yang and Z. Wang, *Anal. Chem.*, 2020, **92**, 14444–14451.
38 W. Chen, Q. Li, W. Zheng, F. Hu, G. Zhang, Z. Wang, D. Zhang and X. Jiang, *Angew. Chem., Int. Ed.*, 2014, **53**, 13734–13739.
39 Z. Li, L. Xu, H. Yuan and P. Zhang, *Analyst*, 2022, **147**, 2930–2935.
40 G. j. Liu, S. n. Tian, C. y. Li, G. w. Xing and L. Zhou, *ACS Appl. Mater. Interfaces*, 2017, **9**, 28331–28338.
41 Y. Yu, W. Ni, Q. Hu, H. Li, Y. Zhang, X. Gao, L. Zhou, S. Zhang, S. Ma, Y. Zhang, H. Huang, F. Li and J. Han, *Angew. Chem., Int. Ed.*, 2024, **63**, e202318483.
42 G. Zhang, Y. Ma, Z. Wang, X. Zhang, X. Wang, S. L. Lo and Z. Wang, *Anal. Chem.*, 2024, **96**, 7787–7796.
43 C. Zhou, W. Xu, P. Zhang, M. Jiang, Y. Chen, R. T. K. Kwok, M. M. S. Lee, G. Shan, R. Qi, X. Zhou, J. W. Y. Lam, S. Wang and B. Z. Tang, *Adv. Funct. Mater.*, 2018, **29**, 1805986.
44 W. Ai, Z. Yang, Y. Ma, X. Han, Y. Chen, K. Zhu and Z. Wang, *Analyst*, 2020, **145**, 6435–6440.
45 H. Yuan, Z. Liu, L. Liu, F. Lv, Y. Wang and S. Wang, *Adv. Mater.*, 2014, **26**, 4333–4338.
46 W. L. Chaffin, J. L. López-Ribot, M. Casanova, D. Gozalbo and J. P. Martínez, *Microbiol. Mol. Biol. Rev.*, 1998, **62**, 130–180.
47 X. M. Han, Y. F. Ma, Y. Z. Chen, X. F. Wang and Z. Wang, *Anal. Chem.*, 2020, **92**, 2830–2838.